Title

Optimized environmental justice calculations for air pollution disparities in Southern California

Journal

Heliyon, 8(10)

ISSN

2405-7843

Authors

Li, Yiting

Kumar, Anikender

Hamilton, Sofia

et al.

Publication Date

2022-10-01

DOI

10.1016/j.heliyon.2022.e10732

Peer reviewed

Heliyon 8 (2022) e10732

Contents lists available at ScienceDirect

Heliyon

journal homepage: www.cell.com/heliyon

Research article

Optimized environmental justice calculations for air pollution disparities in Southern California

Yiting Li [a], Anikender Kumar [b], Sofia Hamilton [c], Jeremy D. Lea [b], John Harvey [b], Michael J. Kleeman [b,*]

[a] Department of Land, Air, and Water Resources, University of California, Davis, CA, USA
[b] Department of Civil and Environmental Engineering, University of California, Davis, CA, USA
[c] Department of Civil and Environmental Engineering, University of Califonria, Berkeley

ARTICLE INFO

Keywords:
Air quality
Environmental disparity
$PM_{2.5}$
Chemical transport model

ABSTRACT

An Environmental Justice (EJ) analysis was carried out using full Chemical Transport Models (CTMs) over Los Angeles, California, to determine how the combination of domain size and spatial resolution affects predicted air pollution disparities in present day and future simulations when data support from measurements is not available. One set of simulations used the Weather Research and Forecasting (WRF) model coupled with Chemistry (WRF/Chem) with spatial resolution ranging from 250 m to 36 km, comparable to census tract sizes, over domains ranging in size from 320 km^2 to 10,000 km^2. A second set of simulations used the UCD/CIT CTM with spatial resolution ranging from 4 km to 24 km over domains ranging in size from 98,000 km^2 to 1,000,000 km^2. Overall WRF/Chem model accuracy improved approximately 9% as spatial resolution increased from 4 km to 250 m in present-day simulations, with similar results expected for future simulations. Exposure disparity results are consistent with previous findings: the average Non-Hispanic White person in the study domain experiences $PM_{2.5}$ mass concentrations 6–14% lower than the average resident, while the average Black and African American person experiences $PM_{2.5}$ mass concentrations that are 3–22% higher than the average resident. Predicted exposure disparities were a function of the model configuration. Increasing the spatial resolution finer than approximately 1 km produced diminishing returns because the increased spatial resolution came at the expense of reduced domain size in order to maintain reasonable computational burden. Increasing domain size to capture regional trends, such as wealthier populations living in coastal areas, identified larger exposure disparities but the benefits were limited. CTM configurations that use spatial resolution/domain size of 1 $km/10^3$ km^2 and 4 $km/10^4$ km^2 over Los Angeles can detect a 0.5 $\mu g\ m^{-3}$ exposure difference with statistical power greater than 90%. These configurations represent a balanced approach between statistical power, sensitivity across socio-economic groups, and computational burden when predicting current and future air pollution exposure disparities in Los Angeles.

1. Introduction

Exposure to outdoor air pollutants such as airborne particles with aerodynamic diameter less than 2.5 μm ($PM_{2.5}$) is estimated to cause 3.3 million premature deaths per year worldwide (Lelieveld et al., 2015). California is home to six out of the ten most polluted cities in the United States with respect to annual-average $PM_{2.5}$ concentrations (American Lung Association, 2019). This air pollution public health burden does not fall evenly across all socio-economic classes, leading to cases of air quality inequity (Anderson et al., 2018). For example, exposure to $PM_{2.5}$ emitted from traffic and power generation is disproportionately higher for people of lower socio-economic status (Anderson et al., 2018; Lelieveld et al., 2015; Thakrar et al., 2020). Many studies have shown that food cooking is a major source of $PM_{2.5}$ (Bond et al., 2007; Butt et al., 2016; Lei et al., 2011; Ramanathan and Carmichael, 2008; Yu et al., 2019), and more recent studies also show that exposure to $PM_{2.5}$ emitted from urban restaurants may be even more skewed than traffic $PM_{2.5}$ (Shah et al., 2020). California is currently enacting climate policies that will lead to a once-in-a-generation improvement in air quality (Kleeman et al., 2013; Zapata et al., 2013, 2017). State law AB32 commits California to reduce GHG emissions to 1990 levels by 2020 (California Air Resource Board, 2006); California Governor's Executive Order S-3-05

* Corresponding author.
E-mail address: mjkleeman@ucdavis.edu (M.J. Kleeman).

https://doi.org/10.1016/j.heliyon.2022.e10732
Received 22 March 2022; Received in revised form 3 August 2022; Accepted 16 September 2022

commits California to an additional 80% reduction below 1990 levels by 2050 (Schwarzenegger, 2005). The latest AB617 is focusing on developing and implementing new strategies to reduce exposure in communities most impacted by air pollution(California Air Resource Board, 2017). It is urgent that an EJ assessment be carried out to ensure that these future benefits are distributed equitably across all members of society. New frameworks are needed to evaluate air quality and Environmental Justice (EJ) in future emissions scenarios.

Understanding the spatial distribution of air pollution fields is a critical first step in any air quality EJ assessment. Exposure fields used in EJ assessment can be obtained from Land Use Regression (LUR) models (Ouyang et al., 2018; Su et al., 2012), dispersion models (Houston et al., 2014), reduced complexity models (Tessum et al., 2019), chemical transport models (CTM) (Izquierdo et al., 2020; Marshall et al., 2014), data fusion methods that incorporate information from air quality monitoring networks and/or satellites (Di et al., 2016; Donkelaar et al., 2019; Hernandez et al., 2021; Kloog et al., 2014; Van Donkelaar et al., 2016) and mobile monitoring networks that produce $PM_{2.5}$ and black carbon fields with high temporal and spatial resolution (Caubel et al., 2019; Chambliss et al., 2021; Deshmukh et al., 2020; Krecl et al., 2020; Messier et al., 2018; Minet et al., 2018). All of these methods can predict historical exposure fields with very high spatial resolution, but only CTMs work as well in future episodes as they do in historical episodes because they are not reliant on data support from historical monitoring data. Reliable future exposure fields are needed to support the increasing demand for future air quality health impact/EJ assessment (Dimanchev et al., 2019; Li et al., 2022; Wang et al., 2020; Zapata et al., 2017).

Measurements show that secondary aerosol formation accounts for approximately 60–80% of $PM_{2.5}$ in California (Heo et al., 2013; US EPA, 1999). The non-linear nature of atmospheric chemical reactions makes the relationships between precursor gas-phase emissions and final ambient particle-phase concentrations complex. Increasing precursor emissions may either increase or decrease the final ambient concentration depending on the chemical regime. CTMs are based on fundamental equations describing atmospheric physics and chemistry, and so they can be used to predict exposure fields in situations where the underlying emissions inventory changes, including scenarios where the atmospheric chemical regime changes from NOx-rich to NOx-limited (Seinfeld and Pandis, 2016). Full CTMs therefore provide the most accurate method to predict future health impacts or EJ analyses in a changing world.

CTMs properly account for complex atmospheric chemistry, but their high computation burden limits their spatial resolution and/or domain size (the size of study area), which can introduce errors into health impact assessments (Fenech et al., 2018; Jiang and Yoo, 2018; Thompson et al., 2014; Thompson and Selin, 2012) and EJ assessment (Paolella et al., 2018). Previous EJ studies in the US have shown that populations with lower socio-economic status are more likely to live near pollution emissions sources and therefore in zones with sharp pollution spatial gradients (Sheppard et al., 1999). Analyzing air pollution exposure in these regions requires high-resolution emissions inventories (Cohan et al., 2006; Markakis et al., 2015; Pan et al., 2017; Tan et al., 2015; Zheng et al., 2017) but even with these inventories in place, the analysis may be limited by the tradeoffs between spatial resolution and domain size. Many studies show that gradients in pollutant concentrations and socio-economic status over intermediate and large spatial scales can be key factors in the analysis of environmental inequity, making the choice of domain size (city-, county-, state-, or national-wide) an important consideration in the EJ assessment (Baden et al., 2007; Chakraborty et al., 2011; Walker, 2009). CTMs applied for EJ assessment therefore need to use a sufficiently large domain size combined with an appropriately fine spatial resolution to capture sharp spatial gradients to bring the critical EJ issues into focus. The goal of this study is to find an appropriate balance between these competing requirements.

CTM computational time and energy consumption generally increase in proportion to the number of active model grid cells (=spatial domain size/grid cell size) in the calculation. The computational burden of CTMs limits their reasonable application to some maximum number of active grid cells. If the resolution of the CTM grid cells increases (smaller cells) then the spatial domain size must decrease to maintain the target number of active cells. Improvements in computational abilities continue to push these limits higher over time, but this factor continues to act as a practical limit to the configuration of CTM studies now and in the near-term future. It is necessary to find a balance between the target domain size and spatial resolution before starting an EJ assessment so that the results are sufficiently reliable and the calculations are computationally efficient. Here we explore how various combinations of (grid resolution x spatial domain size) influence CTM air pollution EJ studies over Southern California. Spatial resolutions ranging from 100's of meters (comparable to census tract levels) up to 36 km are investigated, with associated domain sizes ranging from 320 km^2 to 10,000 km^2. The number of active model grid cells for 4 km, 1 km, and 250 m domains were 27×27, 40×40, and 80×64, respectively. Domains with higher spatial resolution are nested inside of coarse parent domains, and so the time and energy requirements are cumulative. The computational burden normalized to the 4 km domain is 3.2 times higher for the 1 km domain and 10.2 times higher for the 250 m domain. In this study, the ability of each CTM configuration to bring EJ issues into focus is analyzed, and the relationship between spatial resolution, domain size, and statistical power is identified. The results guide the design for future CTM studies to support EJ assessment in California, and the methods provide a roadmap for the design of similar CTM–EJ studies in other regions.

2. Materials and methods

Emissions inventories with spatial resolutions of 36 km, 12 km, and 4 km were first processed with the Sparse Matrix Operator Kernel Emissions (SMOKE) model. Major point sources were specified at their exact latitude and longitude so that these sources can easily be incorporated into fine-scale emissions inventories (1 km/250 m). The locations of area source (non-point source) and mobile emissions inventories were then specified at finer scales using spatial surrogates that were correlated with the true emissions activity. The base year 2016 California Air Resource Board (CARB) emissions inventory (California Air Resources Board, 2019) that served as the starting point for these downscaling calculations used spatial surrogates with a default resolution of 4 km. Emissions are described for six criteria pollutants: PM, NOx, SOx, TOG, CO and ammonia. The emissions within each 1 km/250 m subset of the parent 4 km cell were assigned in proportion to a refined spatial surrogate developed in previous work (Li et al., 2020) as summarized in (Table S1). This methodology is consistent with the standard approach used to downscale county-level emissions to 4 km resolution in the National Emission Inventory (NEI) and CARB emissions inventories. The accuracy of the technique ultimately depends on the accuracy and suitability of the spatial surrogates used to represent the emissions. Further details are provided in the sections below. CARB raw inventories are described at the hourly level using monthly, weekly, and diurnal time profiles for each emission source.

2.1. High resolution area emissions

Fourteen spatial surrogates grouped in seven source categories were used to describe the location of emissions with 1 km/250 m resolution: (1) service and commercial employment and single-family housing (emissions from off-road gasoline engines); (2) off-road construction equipment, farm road vehicle miles travel (VMT), industrial-related/industrial employment (emissions from off-road diesel engines); (3) residential wood burning (emissions from biomass combustion); (4) restaurant sale volume (emissions from food cooking); (5) residential heating gas, industrial-related/industrial employment, service and commercial employment (emissions from natural gas combustion); (6) primary road, secondary road, unpaved road (emissions from road dust); (7) off-road/on-road construction equipment, industrial-related, farm road

VMT, total population (emissions from miscellaneous sources). Surrogate data sources and algorithms are listed in Table S1.

2.2. High resolution mobile emissions

Mobile emissions include both tailpipe emissions and tire/brake wear emissions. Tailpipe emissions can be further divided into gasoline mobile (light-duty vehicles) and diesel mobile (medium- and heavy-duty trucks) by engine type. Surrogates for each of these three subcategories are discussed below.

2.2.1. Gasoline and diesel tailpipe emissions

Explicit traffic counts collected by the U.S. Highway Performance Monitoring System (HPMS) were used to distribute the majority of the tailpipe emissions to highways and other principal arterial roads. McDonald et al. (2014) showed that approximately 70% of gasoline and approximately 80% of diesel vehicle fuel consumption in California occurs on roads with traffic count information. Emissions on these roads can be represented by VMT (i.e., traffic count x road length). The remaining approximately 30% of gasoline and approximately 20% of diesel vehicle activity can use road length as a spatial surrogate. This approximate treatment for the residual portion of the tailpipe emissions should be done separately for urban and rural areas to ensure rural emissions are not overestimated (Brondfield et al., 2012). In California, the approximately 30% of the residual gasoline activity occurs mostly in urban areas (90%) with the balance in rural areas. Data sources can be found in SI Section 1.1. The final mobile gasoline and diesel surrogates were calculated using Eqs. (1) and (2):

$$Surr\ (Gasoline) = 70\% \times (AADT \times Len)_{normalized} + 30\% \times (Len')_{normalized} \quad (1)$$

$$Surr\ (Diesel) = 80\% \times (\ AADT' \times Len)_{normalized} + 20\% \times (Len'')_{normalized} \quad (2)$$

$$Len'' = 90\%\ \times Len\_urban + 10\%\ \times Len\_rural \quad (3)$$

where $Surr\ (Gasoline)$ is the Gasoline mobile surrogate; $Surr\ (Diesel)$ is the Diesel mobile surrogate; AADT is the Annual Average Daily Traffic; AADT′ is the Truck Annual Average Daily Traffic; Len is the Road length with AADT; Len' is the Road length without traffic accounts; Len'' is the Truck road length without traffic accounts, which can be calculated by Eq. (3); Len_urban is the Urban road length; and Len_rural is the rural road length.

2.2.2. Tire and brake wear emissions

Tire and brake wear emissions were estimated as a fixed fraction of tailpipe emissions for all engine types. The CARB SIP 2016 emissions inventories California Air Resource Board, specify that gasoline/diesel emissions account for 86%/14% of total mobile emissions. Thus, the tire and brake wear spatial surrogate was calculated using Eq. (4):

$$Surr\ (Tire\ and\ Brake\ wear) = 86\% \times Surr(Gasoline)_{normalized} + 14\% \times Surr(Diesel)_{normalized} \quad (4)$$

where $Surr\ (Tire\ and\ Brake\ wear)$ is the Tire and Brake wear surrogate.

2.3. Chemical transport model configuration

Annual-average exposure fields over Southern California for the year 2016 were generated using the source-oriented WRF/Chem (SOWC-HR) CTM (Joe et al., 2014; Zhang et al., 2014) coupled with high-resolution emissions inventories summarized above. This version of SOWC used Large Eddy Simulation (LES) to simulate domains with spatial resolution as fine as 250 m. LES predicts turbulent mixing at fine scales where traditional first order closure models are not valid. The Thompson graupel scheme was used for the microphysics option (mp_physics = 8). ACSM2 was used for the boundary-layer option (bl_pbl_physcis = 7). Kain-Fritsch scheme was used for the cumulus option (cu_physics = 1). The SPRAC11 chemical mechanism was used for the gas-phase chemistry option. Multiple domain settings were used (Figure S1) to explore the effects of domain size and spatial resolution. The largest domain with 36 km resolution (D01) covered the entire state of California. A slightly smaller domain with 12 km resolution (D02) covered the South Coast Air Basin (SoCAB). More highly resolved domains with 4 km (D03), 1 km (D04), and 250 m (D05) spatial resolution (employing LES) were nested over Los Angeles. The domain with the highest resolution D05 (250 m) was centered on the community of East Los Angeles, Boyle Heights, West Commerce that has been identified for special study under California's Assembly Bill 617 (AB617). WRF/Chem was configured with two-way nesting between 36 km-12 km–4 km domains and one-way nesting between 4 km-1 km-250 m domains.

A second set of exposure fields was also developed using the University of California Davis/California Institute of Technology (UCD/CIT) CTM (Kleeman and Cass, 2001). The UCD/CIT model was configured with one parent 24 km statewide domain and one nested 4 km domain covering the SoCAB (Figure S1). One-way nesting was used between the domains. UCD/CIT model simulations employed a different set of emissions inventories. Primary dust emissions used by the WRF/Chem model are higher than the dust emissions used by the UCD/CIT model. Comparison of the concentration fields predicted by both models suggests that different dust emissions can account for a change in predicted $PM_{2.5}$ mass concentrations of approximately 1.5 μg m^{-3}. The UCD/CIT model used standard 4 km CARB mobile emissions developed using travel demand models combined with the EMFAC model. The WRF/Chem model used mobile emissions with 1km spatial resolution developed using the methods summarized in Section 2.2. In addition to having different spatial resolutions, the different approaches used to develop these inventories yield slightly different spatial patterns for the mobile emissions. Results from WRF/Chem and the UCD/CIT model will be compared to identify common trends.

2.4. Socio-economic data

Socio-economic data were obtained from the American Community Survey (ACS) 2012–2016 (United State Census Bureau, 2020). The dataset describes four race/ethnicity groups that were analyzed in detail in the current study: Black (Black and African American alone), Hispanic (Hispanic or Latino, regardless of race), Asian (Asian alone), and non-Hispanic White (White, not Hispanic or Latino). Population maps for these race/ethnicity groups are shown in Figures S2 and S3 with a summary for each model domain presented in Table S2. The Hispanic fraction of the population increases as the model domains becomes more focused on central Los Angeles, rising from 38% in D01 to 67% in D05. Conversely, the Non-Hispanic White fraction of the population decreases steadily from 38% in D01 to 10% in D05. Asian (13–16%) and Black and African American (6–10%) population fractions are more constant across the model domains D01 through D05. The ACS dataset also includes seven income categories spanning the range from less than 50% of the poverty level to greater than twice the poverty level. Income distributions across the model domains D04 and D05 are summarized in Table S3. Intermediate income levels are similar across domains, but 28% of the population in D05 is below the poverty level compared to 20% in D04, and only 42% of the population is more than 2× above the poverty level in D05 compared to 57% in D04. These statistics illustrate that the inner D05 modeling domain employed in the current study contains a larger fraction of the poorest population. D05 is a subset of D01–D04, but the larger regions contain areas with cleaner air and a higher proportion of white residents. Thus, analysis carried out over D01–D04 dilutes the disparities experienced by the poorest residents.

EJ assessments were done for nine combinations of domain size and spatial resolution, including D01–36 KM, D02—12 KM, D03—12 KM,

D03—4 KM, D04—4 KM, D04—1 KM, D05—4 KM, D05–1 KM and D05—250 M. The domain size-resolution combinations selected for analysis were constrained by the computational burden at fine spatial resolution and sufficiently large sample size at coarse resolution. Fine-scale domains with more than 10,000 grid cells were not used in order to maintain reasonable computational burden. Coarse-scale domains with fewer than 20 grid cells were not used to maintain sufficiently large sample size.

Socio-economic data with census tract resolution were used for the analysis. Within the primary study region (Los Angeles D02), 51% of census tracts are below 1 km resolution and 72% of census tracts are below 1.2 km resolution. A histogram of census tract size is shown in Figure S4. The resolution of the socio-economic data is well matched with the resolution of the model domains in the current study. Population data used in EJ assessment were regirded into spatial resolutions that were comparable to the CTM exposure fields.

Population weighted concentration were calculated for four race/ethnicity groups and two poverty level categories. Both absolute disparity and relative disparity were analyzed. Relative disparity results are expressed as the percentage difference relative to the total population average ($(PWC_{race/income} - \overline{PWC}) / \overline{PWC} * 100\%$).

2.5. Statistical power

EJ assessments were performed using several combinations of domain size and spatial resolution. Statistical power was used as a metric to evaluate the capability of each combination to detect a given disparity value and therefore to determine whether the combination of domain size and spatial resolution was suitable for future studies. Statistical power is calculated using standard statistical procedures involving Type II error during a test of the means in two samples. Type II error occurs when the null hypotheses is not rejected even though it is false. A lower probability of a Type II error (β) generates a higher statistical power ($1 - \beta$), which can be interpreted as a more sensitive test. Statistical power and Type II error for tests of the means are related to four parameters: mean of two samples (two races/ethnicities or two income groups); standard deviation of two samples; sample size, and Alpha level (α), which were provided in SI Section 2.3. We chose $\alpha = 0.01$ in this study. The statistical power results are presented in Section 3.4.

3. Results and discussion

3.1. CTM exposure fields and model performance

Figure 1(a, b, c, d) shows the annual mean $PM_{2.5}$ mass concentration predicted by WRF/Chem in the year 2016 at spatial resolutions of 12 km (D02, Figure 1(a)), 4 km (D03, Figure 1(b)), 1 km (D04, Figure 1(c)) and 250 m (D05, Figure 1(d)). Annual mean concentrations of $PM_{2.5}$ Elemental Carbon (EC), $PM_{2.5}$ Organic Carbon (OC), $PM_{2.5}$ primary aerosol mass, and $PM_{2.5}$ secondary aerosol mass are shown in Figures S5—S8. Thin gray lines in Figure 1 panels b,c,d represent state highways, black lines in panels a, b, c represent California GAI

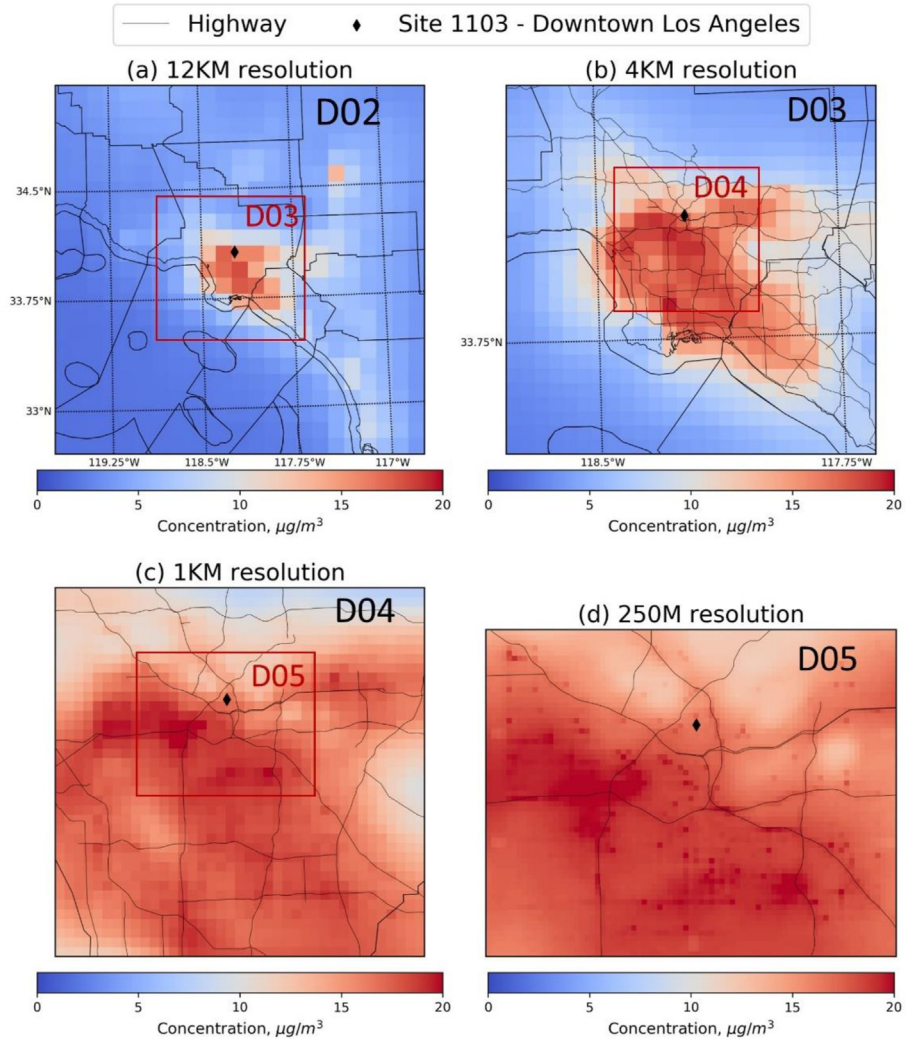

Figure 1. Year 2016 predicted annual mean $PM_{2.5}$ mass concentration ($\mu g/m^3$) at 12 km (a), 4 km (b), 1 km (c), 250 m (d) spatial resolution.

(Geographic Area Index) boundaries, which combine county boundaries and air basin boundaries. Pollutants with shorter atmospheric lifetimes (such as primary particles) have concentrations that rapidly decay downwind of emissions locations (Karner et al., 2010). Higher spatial resolution therefore reveals sharper concentration spatial gradients around major traffic corridors and large stationary emissions sources. Maximum concentrations and the number of "hotspots" both increase with finer spatial resolution in Figure 1, yielding a more complex exposure field that captures the influence of both local sources as well as regional background concentrations.

Figure 2(a, b, c, d) shows annual-mean concentrations of $PM_{2.5}$ EC, $PM_{2.5}$ OC, $PM_{2.5}$ primary mass, and $PM_{2.5}$ secondary mass predicted at 1 km (D04) and 250 m (D05) spatial resolution. Figure 2 shows that $PM_{2.5}$ EC concentrations are elevated around major transportation corridors, with sharper spatial gradients coming into focus at finer spatial resolution (Figure 2(a), D04 vs. D05). Increased $PM_{2.5}$ EC concentrations can also be observed around major surface streets at 250 m resolution (Figure 2(a), D05). Predictions at 12 km and 4 km spatial resolution are too coarse to detect elevated $PM_{2.5}$ EC concentrations adjacent to highways or major roadways, but these coarser predictions do still capture the general increase over the urban area (Figure S5). $PM_{2.5}$ OC concentration fields are smoother than $PM_{2.5}$ EC concentration fields at all spatial resolutions (Figure 2(b) vs. Figure 2(a) and Figure S6 vs. Figure S5). Primary $PM_{2.5}$ OC (Figure 2(b)) is emitted by a larger number of sources (food cooking, traffic, biomass combustion) than $PM_{2.5}$ EC (primarily traffic) in the current simulations. Secondary reactions in the atmosphere also produce $PM_{2.5}$ OC over periods of hours to days, which smooths the resulting concentration fields. Primary $PM_{2.5}$ mass (Figure 2(c)) consisting of EC, primary OC, metals, and other crustal elements responds to spatial resolution similarly to EC, with sharper spatial gradients revealed at higher resolution. In contrast, secondary $PM_{2.5}$ mass (Figure 2(d) and Figure S8) has relatively smooth spatial gradients that do not change significantly as spatial resolution is increased. The overall results illustrated in Figure 2(a, b, c, d) show that finer spatial resolution captures the sharp gradients associated with primary pollutants such as EC but reveals few additional features for secondary aerosol.

Predicted concentrations of $PM_{2.5}$ mass, $PM_{2.5}$ EC, and $PM_{2.5}$ OC were compared to all available measurements during the study period (Figures S12 and S13). Daily $PM_{2.5}$ mass, Mean Fractional Bias (MFB) and Mean Fractional Error (MFE) of the CTM predictions at 12 km, 4 km, 1 km and 250 m are calculated at ten available sites. Daily $PM_{2.5}$ EC, OC MFB and MFE are calculated at one site (downtown Los Angeles). Monthly mean/daily predicted and measured $PM_{2.5}$ mass, $PM_{2.5}$ EC, $PM_{2.5}$ OC at Downtown Los Angeles site are shown in SI (Figure S10 and Figure S11). In general, simulations at all spatial resolutions capture time trends in $PM_{2.5}$ mass, $PM_{2.5}$ EC, and $PM_{2.5}$ OC concentrations. $PM_{2.5}$ mass, $PM_{2.5}$ EC, $PM_{2.5}$ OC were slightly over predicted in summer months due to an under prediction of wind speed. All MFB are $\leq$60% and MFE values are $\leq$75%, meeting typical CTM performance criteria(Boylan and Russell, 2006). Three out of four sites that used 1 km spatial resolution met typical CTM performance goals(Boylan and Russell, 2006) (MFB $\leq$30% and MFE $\leq$50%). Model performance (both MFB and MFE) improved by 5% when the spatial resolution was increased from 4 km to 1 km; model performance improved an additional 4% when the spatial resolution was increased from 1 km to 250 m. It is noteworthy that model performance degrades slightly as spatial resolution increases from 12 km to 4 km, and then improves as spatial resolution increases from 4 km to 1 km to 250 m at the available measurement sites. UCD/CIT Model performance is summarized in Figure S9. UCD/CIT model results meet typical CTM performance goals (Boylan and Russell, 2006) (MFB $\leq$30% and MFE $\leq$50%) for all available measurement sites.

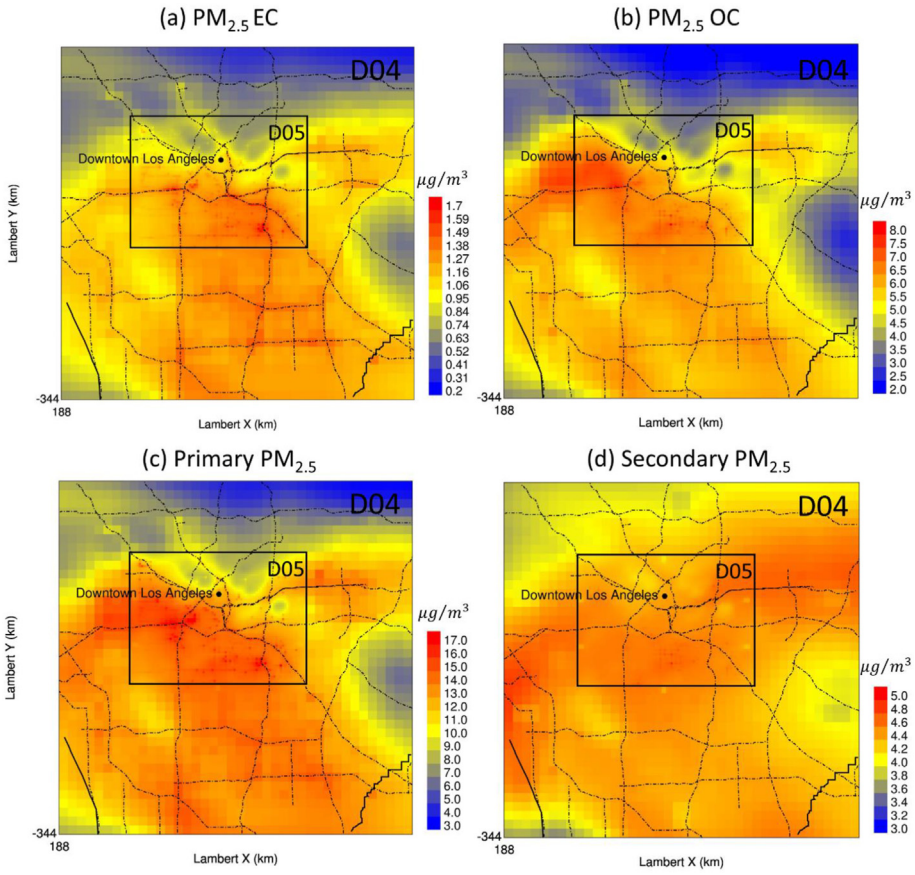

Figure 2. Year 2016 annual mean $PM_{2.5}$ EC, $PM_{2.5}$ OC, $PM_{2.5}$ primary, and $PM_{2.5}$ secondary aerosol mass concentration ($\mu g/m^3$) at 1 km (domain D04) and 250 m (domain D05) spatial resolution. Dashed line is state highway.

Model performance as a function of location was analyzed by comparing annual-mean predicted concentration to measurements across the study domain as recommended by Paolella et al. (2018) The reasonably high correlation coefficient calculated in this analysis (R^2 = 0.61 in Figure S14) shows that predicted concentration fields have a spatial pattern that is consistent with measured concentrations.

While the CTM error analysis builds confidence in the accuracy of the overall modeling system, it does not address the key issue of the appropriate combination of domain size and spatial resolution to capture a sufficiently large population with enough concentration contrast to best support epidemiological studies.

3.2. EJ analyses at different CTM domain size and spatial resolution

Results are stratified by the population socio-economic class information available in the public ACS datasets. Annual-average population-weighted concentrations (PWC) of $PM_{2.5}$ mass, $PM_{2.5}$ EC, $PM_{2.5}$ OC, $PM_{2.5}$ primary mass, and $PM_{2.5}$ secondary mass are calculated to represent exposures for each socio-economic group across all CTM domains and spatial resolutions (Figure S15 for race-income D04, 05, Figure S16 for race-income D01,02,03, Figure S17 for income alone D04-D05).

Absolute and relative disparities of $PM_{2.5}$ mass and its components were calculated across all WRF/Chem CTM domains and for their intersection with UCD/CIT CTM domains, including statewide 24 km, 4 km on D03 (UCD/CIT, D03-4 KM), and 4 km on D04 (UCD/CIT, D04-4KM). UCD/CIT results were developed independently from WRF/Chem results and so they serve as a comparison group to identify trends common across model platforms.

In general, Los Angeles residents in lower socio-economic groups are predicted to experience higher exposure to air pollutants, especially primary pollutants, regardless of CTM domain size and spatial resolution. This finding is consistent with the results from previous studies over Los Angeles (Cushing et al., 2015; Paolella et al., 2018; Tessum et al., 2019). However, the current study predicts that exposure to secondary $PM_{2.5}$ mass was similar across all races and income categories. Below we discuss further details of the combined effects of CTM domain size and spatial resolution on the EJ results and the statistical power of the analysis.

3.2.1. Absolute disparity

Figure 3(a and b) summarizes the exposure difference between the largest disparity groups across all combinations of CTM domain size and resolution as a function of race-income (Figure 3(a)) and income alone (Figure 3(b)). The largest absolute disparity in the current study was observed between low-income Black and African American and high-income non-Hispanic White groups, except at the statewide domain level D01, 36 km (see caption in Figure 3(a)). Observed race-income related maximum exposure disparities were 1.63–5.18 $\mu g/m^3$ for $PM_{2.5}$ mass; 0.12 to 0.4 $\mu g/m^3$ for $PM_{2.5}$ EC; 0.63 to 2.0 $\mu g/m^3$ for $PM_{2.5}$ OC; 1.25 to 4.25 $\mu g/m^3$ for primary mass; 0.12 to 0.75 $\mu g/m^3$ for $PM_{2.5}$ secondary. The choice of model domain size at a constant resolution changed calculated absolute disparity values by 12%–28%. The choice of model spatial resolution at a constant domain size changed calculated absolute disparity values by 1%–6%. Changing the domain size has relatively larger effect on absolute disparity. Note that income level did not have a statistically significant effect on air pollution exposure over

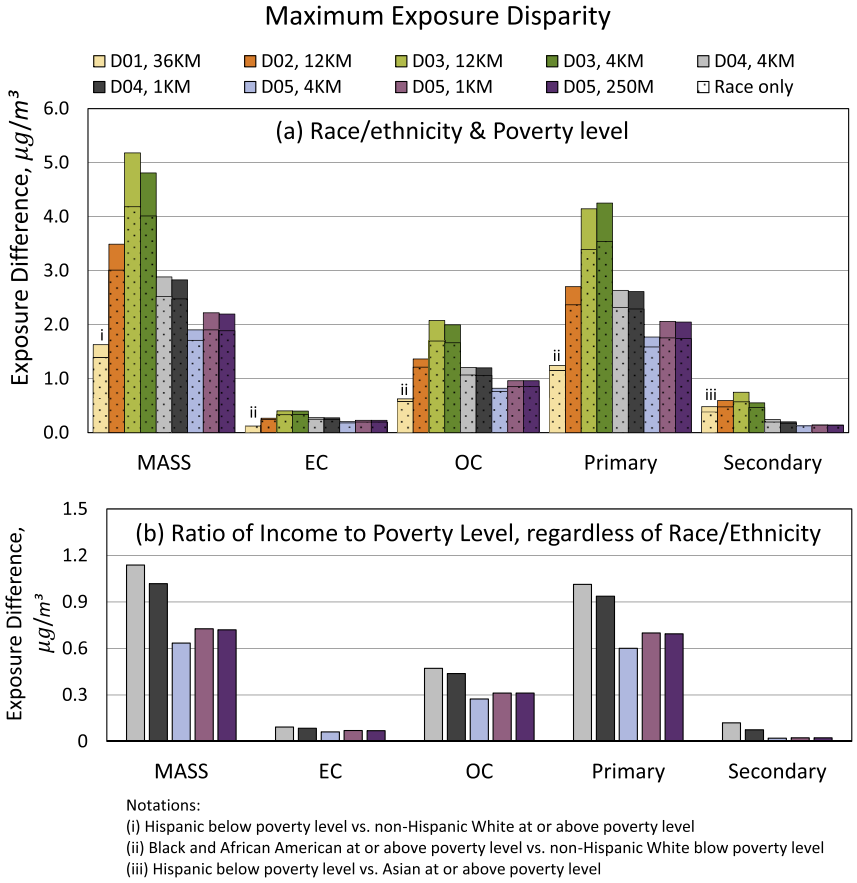

Figure 3. Pollutant exposure difference between the maximum disparity groups. All species analyzed here are in the $PM_{2.5}$ size fraction. Comparison groups in (a) are Black and African American below poverty level vs. non-Hispanic White above poverty level except for D01, 36 KM result. Comparison groups in panel (b) are people who are less than 0.5× the poverty level vs. people who are more than 2× the poverty level. CTM domains are shown in Figure S1.

the largest domain (D01) that employed the coarsest spatial resolution. When exposures were analyzed without regard to income level, the maximum disparity between race groups decreased approximately 8% (D01) to 18% (D04) (shaded area in Figure 3(a)).

Absolute exposure disparities between different racial groups calculated by WRF/Chem and the UCD/CIT model are compared across statewide, D03-4KM, and D04-4KM domains in Figure S19. The trends in exposure disparity as a function of domain size and domain resolution are consistent between the two CTM predictions. Absolute values of exposure disparities calculated with the models are in better agreement when over-predictions in dust emissions in the WRF/Chem model were subtracted from the predicted concentration fields. The agreement between results produced by these independent models builds confidence in the exposure disparities identified in the current study.

Hypothesis tests were conducted for population-weighted $PM_{2.5}$ mass exposures across race and poverty levels to further investigate poverty-related disparity. The population-weighted exposures are calculated with a finite number of grid cells with a total count that is far smaller than the number of people in the study region. The calculated population exposure can therefore be viewed as a sub-sample of the individualized population exposure (that is impractical to calculate). Test statistics were calculated using the weighted mean and the weighted standard deviation for each population exposure across all available model grid cells (summarized in Tables S4–S8). Further details of the calculation approach are provided in SI Section 2.3 and in SI Tables S9–S10. P-values were calculated to test the hypothesis that each paired comparison group had the same exposure. Three stratifications were considered: (i) combined race and poverty level; (ii) race only; and (iii) poverty level only. Statistically significant maximum exposure disparities (p-values $< 1\%$) were identified in most CTM configurations when considering race and poverty level together or race alone, except for the comparison between low-income Asian and high-income White groups. The dependence on CTM domain size and spatial resolution became more apparent when testing the smaller effects of poverty alone. Statistically significant differences by poverty level were only detected at higher resolution regional/community-level domain (4 km at D03, 1 km at D04 and 250 m at D05) that had sufficient combined size and resolution. All of the subsequent tests involving income levels will focus on regional/community-level domains in order to maintain statistical power at a meaningful level.

The largest air pollution exposure disparities based on income occur between the highest and the lowest income categories, but the maximum income exposure disparities (Figure 3(c)) were approximately 50% smaller than maximum race exposure disparities (shaded bar in Figure 3(a)) over the income categories tested. The effect of income was further analyzed by comparing exposure disparities between households with income greater than $200,000/yr and households with income below $10,000/yr in D03, D04, and D05 (see Table S11). Exposure disparity for $PM_{2.5}$ mass is 1.5–4 times higher when comparing these more divergent income categories, with similar increases for the exposure disparities in the components of $PM_{2.5}$ mass. These results suggest that income is an important factor in air pollution exposure disparity, but it must be recognized that income and race are often highly correlated (see Paolella et al., 2018 for discussion on this topic). More than 80% of the households with income greater than $200,000/yr in the current study are non-Hispanic White, making it is difficult to separate income vs. race contributions to exposure disparity.

Figure 3(a and b) illustrates how maximum exposure disparity for primary and secondary PM responds to CTM domain size and spatial resolution. The largest statewide domain (D01) has the lowest maximum exposure disparity for primary PM due to the corresponding coarse spatial resolution. In contrast, exposure disparities for secondary PM increase with domain size regardless of spatial resolution since spatial gradients for secondary pollutants occur over larger distances. Maximum exposure disparity for all $PM_{2.5}$ mass and components increased from source-oriented WRF/Chem statewide D01 to region-level D03, then decreased from D03 to D05.

Two trends are apparent when comparing results with different spatial resolutions but the same domain size (D03, 04, and D05) in Figure 3. Within the community-level domain (D05), the exposure disparity increased with spatial resolution (4km, 1km, 250m). The opposite trend is observed in the regional domain (D03 and D04), where the exposure disparity slightly decreased with spatial resolution (12km, 4km, 1km). D03 and D04 include more coastal areas that inherently have lower exposures because they have fewer upwind sources. Thus, analysis conducted in D03 and D04 captures the increased disparity between those who live closer to the coast (non-Hispanic White or wealthy people) and those who live in inland (other non-White categories). In this case, the effects of the larger domain size overwhelm the effects of the higher spatial resolution.

3.2.2. Relative disparity

Figure 4(a, b, c, d, e, f) illustrates deviations from the total population average concentrations estimated for each socio-economic group for $PM_{2.5}$ total mass, $PM_{2.5}$ primary mass, and $PM_{2.5}$ secondary mass (similar results for $PM_{2.5}$ EC and OC are presented in Figure S18). Overall, Black and African American and Hispanic residents experience higher than average exposure to $PM_{2.5}$ total mass (2%–23%) and to $PM_{2.5}$ secondary aerosol (1%–10%); Non-Hispanic White and Asian residents experience lower than average exposure to $PM_{2.5}$ total mass (4%–13%) and to $PM_{2.5}$ secondary aerosol (1%–6%). People with income lower than twice the poverty level generally experience similarly higher air pollution exposures, whereas people with income more than twice the poverty level experience lower air pollution exposure. Further refinement of income categories at higher levels would likely reveal even greater levels of exposure disparity.

Relative exposure disparities between different racial groups calculated by WRF/Chem and the UCD/CIT model are compared across statewide, D03-4 KM, and D04-4 KM domains with results provided in Figure S20. Trends in exposure disparities across different racial groups are in strong agreement between the two model predictions. Black and African American and Hispanic residents consistently have higher than average exposure to total $PM_{2.5}$, while non-Hispanic White residents consistently have lower than average exposure. Asian residents have exposure levels that are very close to average. The biological significance of the $PM_{2.5}$ exposure disparities can be quantified using the methods that are used to estimate the public health burden of air pollution exposure. The mortality risk ratio (RR) associated with air pollution exposure is often represented using Eq. (5):

$$RR = e^{\beta\left(C_{exposure} - C_{background}\right)} \tag{5}$$

where C_exposure is the exposure concentration and C_background is the background concentration for the pollutant of interest. Krewski et al. (2009) performed a follow-up analysis of the American Cancer Society (ACS) cohort and derived a β value of 1.036 for exposure to $PM_{2.5}$ mass. Applying Eq. (5) to the population-weighted-concentrations experienced by each racial group in domain D04-4KM yields a risk ratio for Black and African American residents that is approximately 30% higher than the risk ratio for the Non-Hispanic White group. It should be noted that the risk ratio calculation is non-linear and so a more exact treatment would apply Eq. (5) separately for residents in different exposure bands and then combine the results. The current analysis provides a rough estimate of health impacts, with a more exact treatment described in other work (see for example Li et al., 2022).

CTM domain size and spatial resolution combine to influence the exposure disparities illustrated in Figures 3 and 4. Maximum exposure disparities generally come into clearest focus when intermediate combinations of domain size and spatial resolution are used since this balanced configuration captures exposure gradients for both primary and

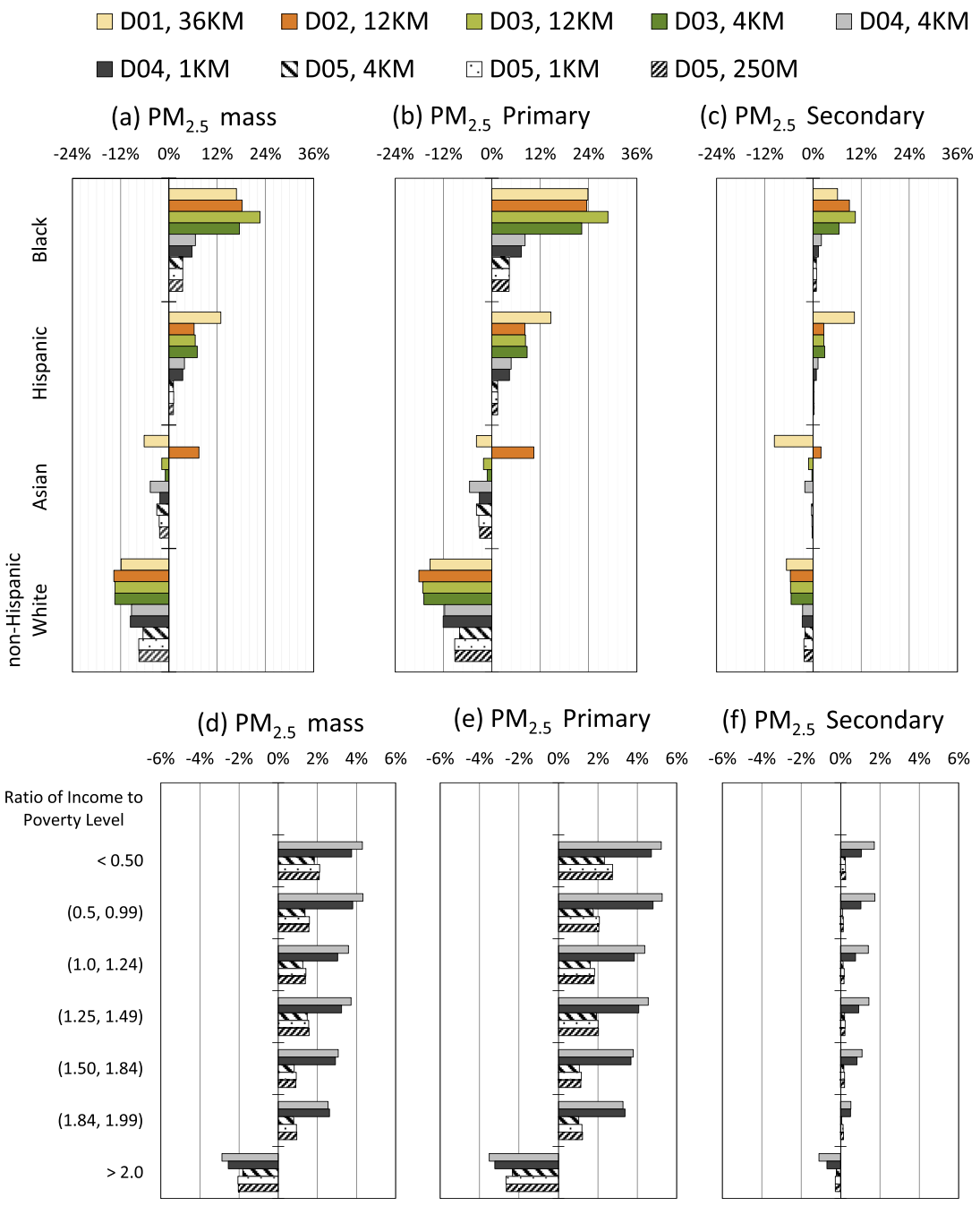

Figure 4. Exposure difference relative to population average for (a,d) $PM_{2.5}$ mass, (b,e) primary $PM_{2.5}$ mass, and (c,f) secondary $PM_{2.5}$ mass as a function of domain size and resolution. Upper panels analyze race/ethnicity and lower panels analyze income.

secondary PM. The exception to this finding in the current study is that Hispanic exposure disparities were highest in the largest domain (D01) that covered the entire state of California. Results for exposure disparity based on income shown in the lower panels of Figure 4 do not include the largest spatial domain because these findings were not statistically significant (see Tables S9-S10 and associated discussion), but the intermediate combinations of domain size and spatial resolution once again bring the largest exposure disparities into clearest focus.

The asymmetry of the exposure disparities in Figure 4(a, b, c, d, e, f) are noteworthy. Within larger domains (D01-D03), the maximum exposure disparities based on race were +23% for the highest exposure group and −13% for the lowest exposure group. Within smaller domains (D04-405), the asymmetry pattern reversed, with +6% for the highest exposure group and −10% for the lowest exposure group based on race. Similar asymmetry patterns were observed for maximum exposure disparities based on income: +4% for the highest exposure group and −3% for the lowest exposure group within the larger domain D04. Smaller but similar deviations (+2%/−2%) were observed for the highest and lowest exposure groups within the smaller domain D05. This asymmetry was largely driven by exposure to primary PM, with substantially lower exposure disparities associated with secondary PM. Smaller domains have higher average concentrations that can reduce the maximum exposure disparities. The combined trends illustrated in Figures 3 and 4 emphasize the need for a balanced selection of domain size and spatial

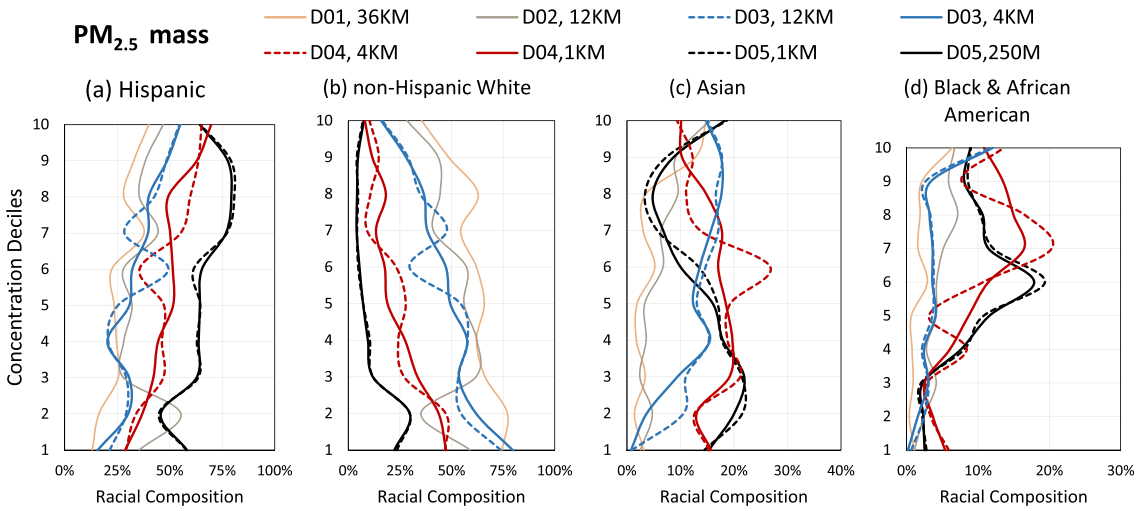

Figure 5. $PM_{2.5}$ mass exposure distribution across racial-ethnic population. (a), (b), (c), (d) focus on spatial resolution and domain scope changes on racial-ethnic population exposure distribution. Population profile at a given concentration level can be found by following a horizontal line across each sub-panel and comparing results from lines with the same color across panels.

resolution when quantifying exposure disparities, with slightly higher priority given to selection of a sufficiently large domain to represent the large-scale exposure features. Increasing the spatial resolution beyond approximately 1 km appears to produce diminishing returns in the current study.

3.3. Exposure distribution

Figure 5(a, b, c, d) illustrates the distribution of $PM_{2.5}$ mass exposure disparities across different race/ethnicity groups as a function of the CTM domain and spatial resolution. Calculations using different CTM domain size and spatial resolution are shown as different colors within each panel of Figure 5. Exposure distributions are divided into concentration deciles and exposures for each race/ethnicity group are expressed on a relative scale within each decile. Similar exposure distributions for $PM_{2.5}$ EC, $PM_{2.5}$ OC, $PM_{2.5}$ primary mass and $PM_{2.5}$ secondary mass are presented in the SI (Figure S21). The results in Figure 5 and Figure S21 illustrate which race/ethnicity groups experience the highest and lowest PM exposures in California. For reference, the $PM_{2.5}$ mass racial/ethnicity compositions of absolute concentration deciles for each domain-resolution combination are shown in Figure S22. It should be noted that each race/ethnicity group comprises a different fraction of domain total population, and so it is not expected that exposure distributions would be equal when comparing between race/ethnicity groups. Rather, the most equitable distribution of exposures in Figure 5(a, b, c, d) would be for each race/ethnicity group to have relatively uniform exposure across all concentration deciles (straight vertical line).

The sloped exposure distributions illustrated in Figure 5(a, b, c, d) reflect the disparities discussed in the previous sections. Results vary slightly with domain size, but Hispanic and Black and African American racial groups experience increased exposure to the highest deciles of PM concentration while the non-Hispanic White group experiences lower exposure to the highest concentration. Balanced combinations of domain size and domain resolution once again bring the disparities (slope of each line) into sharpest focus. Domain size generally does not change the slope of the exposure distribution lines for Hispanic and non-Hispanic White groups because their populations are distributed more uniformly across California (De La Cruz-Viesca et al., 2016). Domain size has a larger influence on the shape and slope of the exposure distribution lines for Asian and Black and African American groups because these populations are more concentrated in urban areas.

Figure 5 shows that lower spatial resolution, especially 4 km, 12 km and 36 km, generates larger fluctuations across the exposure distribution because the coarse resolutions cannot adequately resolve the combined population and concentration spatial gradients. A larger grid cell incorporates a larger fraction of the population into one decile. Breaking large grid cells into small grid cells divides the same population among multiple concentration deciles resulting in a smoother (and more realistic) exposure distribution. This same issue will influence the calculated average exposure for each socio-economic group shown in Figures 3 and 4, emphasizing the need for a sufficiently fine spatial resolution to resolve EJ issues.

3.4. Statistical power

The analysis presented in the previous sections shows that CTM calculations for EJ assessment that balance both domain size and spatial resolution in the context of race and income patterns can obtain meaningful results with reduced computational burden. This finding is illustrated with an example in Figure 6 showing the statistical power of different CTM configurations over Southern California to correctly identify $PM_{2.5}$ mass exposure disparities between groups in cases where

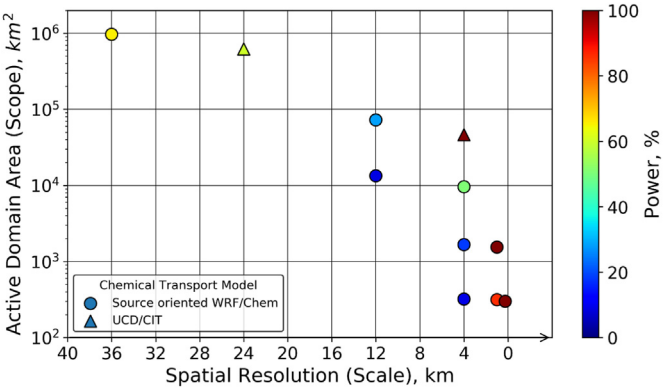

Figure 6. Power of detecting a 0.5 $\mu g/m^3$ maximum exposure disparity between groups for each combination of spatial resolution and domain scope, including both source oriented WRF/Chem (dot) and UCD/CIT (triangle) CTM results. A power of 90% indicates that there is a 90% probability of correctly concluding that exposures are different between the groups.

the true disparity is 0.5 μg/m^3. The horizontal axis of Figure 6 represents increasing spatial resolution to the right, while the vertical axis represents increasing active domain area (CTM grid cells with non-zero population) towards the top. Statistical power to detect the indicated concentration difference between maximum disparity groups is shown as color, with statistical power above 90% shown in red. Figure 6 shows that EJ statistical power can be increased by either increasing the domain size or increasing the spatial resolution. Achieving statistical power above 90% in our target area requires 4 km spatial resolution with a domain size greater than 10^4 km^2, 1 km spatial resolution with domains size greater than 10^3 km^2, or 250 m spatial resolution with domain size greater than 10^2 km^2.

4. Conclusions

Increasing the spatial resolution of CTM calculations should increase the accuracy of the predicted concentration fields. In the current study, simulations with higher spatial resolution were able to better resolve sharp spatial gradients downwind of major transportation corridors and large point sources. Model performance improved by approximately 5% when the spatial resolution was increased from 4 km to 1 km; model performance improved an additional approximately 4% when the spatial resolution was increased from 1 km to 250 m. This overall approximately 9% increase in model performance must be weighed against the need to reduce the spatial domain size from approximately 10,000 km^2 (4 km resolution) to approximately 320 km^2 (250 m resolution) in order to keep the computation burden manageable. The limited coverage of the 250 m simulations reduces the population in the study region and it prevents an analysis of the concentration gradients that occur over lengths of 100's of km.

Environmental disparities by race/ethnicity groups and poverty groups were done at nine resolution-domain combinations. A regional analysis with 4 km or 1 km spatial resolution appears to bring EJ issues into focus across the different scales in Southern California. In the current study, 4 km spatial resolution with a domain size greater than 10^4 km^2 or 1 km spatial resolution with domains size greater than 10^3 km^2 identify $PM_{2.5}$ exposure disparities as large as 17.5% that translates into a 30% increase in the mortality risk ratio. The air pollution domains balance the accuracy of model predictions vs. measurements, they include populations in all important subregions, and they maximize the accuracy of the exposure distributions across all socio-economic groups.

The statistical power for each domain-resolution combination calculated in the current study is determined by the spatial distribution of pollution and the demographics of regional housing patterns within each domain. The shape of the relationship between statistical power vs. domain-resolution identified in the current study is expected to be typical for other regions, but the exact thresholds for achieving a target level of statistical power at a relevant level of exposure disparity will need to be recalculated for each new study domain. The current study provides a single data point that fine-scale spatial resolution below 1km may not be needed (or even optimal if it requires diminished domain size). Similar studies should be carried out in other geographic regions in order to determine the appropriate CTM domain size and spatial resolution for EJ assessment in the context of their spatial distributions for race and income.

Declarations

Author contribution statement

Yiting Li: Performed the experiments; Analyzed and interpreted the data; Wrote the paper.

Anikender Kumar; Sofia D Hamilton; Jeremy D Lea; John Harvey: Contributed reagents, materials, analysis tools or data.

Michael J Kleeman: Conceived and designed the experiments; Analyzed and interpreted the data; Wrote the paper.

Funding statement

This work was supported by U.S. Environmental Protection Agency [R83587901].

Data availability statement

Data will be made available on request.

Declaration of interest's statement

The authors declare no conflict of interest.

Additional information

Supplementary content related to this article has been published online at https://doi.org/10.1016/j.heliyon.2022.e10732.

Acknowledgements

Although the research described in the article has been funded by the United States Environmental Protection Agency it has not been subject to the Agency's required peer and policy review and therefore does not necessarily reflect the reviews of the Agency and no official endorsement should be inferred.

References

American Lung Association, 2019. State of the Air 2019 [WWW Document]. URL. https://www.stateoftheair.org/assets/sota-2019-full.pdf.

Anderson, C.M., Kissel, K.A., Field, C.B., Mach, K.J., 2018. Climate change mitigation, air pollution, and environmental justice in California. Environ. Sci. Technol. 52, 10829–10838.

Baden, B.M., Noonan, D.S., Turaga, R.M.R., 2007. Scales of justice: is there a geographic bias in environmental equity analysis? J. Environ. Plan. Manag. 50, 163–185.

Bond, T.C., Bhardwaj, E., Dong, R., Jogani, R., Jung, S., Roden, C., Streets, D.G., Trautmann, N.M., 2007. Historical Emissions of Black and Organic Carbon Aerosol from Energy-Related Combustion, 1850–2000. Global Biogeochem. Cycles 21.

Boylan, J.W., Russell, A.G., 2006. PM and light extinction model performance metrics, goals, and criteria for three-dimensional air quality models. Atmos. Environ. 40, 4946–4959.

Brondfield, M.N., Hutyra, L.R., Gately, C.K., Raciti, S.M., Peterson, S.A., 2012. Modeling and validation of on-road CO2 emissions inventories at the urban regional scale. Environ. Pollut. 170, 113–123.

Butt, E.W., Rap, A., Schmidt, A., Scott, C.E., Pringle, K.J., Reddington, C.L., Richards, N.A.D., Woodhouse, M.T., Ramirez-Villegas, J., Yang, H., Vakkari, V., Stone, E.A., Rupakheti, M., Praveen, S., van Zyl, G., Beukes, P.,P., Josipovic, M., Mitchell, E.J.S., Sallu, S.M., Forster, P.M., Spracklen, D.V., 2016. The impact of residential combustion emissions on atmospheric aerosol, human health, and climate. Atmos. Chem. Phys. 16, 873–905.

California Air Resource Board, 2017. Assembly Bill No. 617 Nonvehicular Air Pollution: Criteria Air Pollution and Toxic Air Contaminants [WWW Document]. URL. https://leginfo.legislature.ca.gov/faces/billTextClient.xhtml?bill_id=201720180AB617.

California Air Resource Board, 2006. Assembly Bill No. 32: Air Pollution: Greenhouse Gases: California Global Warming Solutions Act of 2006 [WWW Document]. URL. https://leginfo.legislature.ca.gov/faces/billTextClient.xhtml?bill_id=200520060AB32.

California Air Resource Board. n.d. California Air Resource Board SIP 2016 Emissions Projection Data [WWW Document]. URL. https://www.arb.ca.gov/app/emsinv/2017/emssumcat_query.php?F_YR=2012&F_DIV=-4&F_SEASON=A&SP=SIP105ADJ&F_AREA=CA#AREAWIDE.

California Air Resources Board, 2019. CEPAM2019v1.03 - Standard Emission Tool [WWW Document]. URL. https://ww2.arb.ca.gov/applications/cepam2019v103-standard-emission-tool.

Caubel, J.J., Cados, T.E., Preble, C.V., Kirchstetter, T.W., 2019. A distributed network of 100 black carbon Sensors for 100 Days of air quality monitoring in west Oakland, California. Environ. Sci. Technol. 53, 7564–7573.

Chakraborty, J., Maantay, J.A., Brender, J.D., 2011. Disproportionate proximity to environmental health hazards: methods, models, and measurement. Am. J. Public Health 101, S27–S36.

Chambliss, S.E., Pinon, C.P.R., Messier, K.P., LaFranchi, B., Upperman, C.R., Lunden, M.M., Robinson, A.L., Marshall, J.D., Apte, J.S., 2021. Local- and regional-scale racial and ethnic disparities in air pollution determined by long-term mobile monitoring. Proc. Natl. Acad. Sci. U. S. A. 118, e2109249118.

Cohan, D.S., Hu, Y., Russell, A.G., 2006. Dependence of ozone sensitivity analysis on grid resolution. Atmos. Environ. 40, 126–135.

Cushing, L., Faust, J., Meehan August, L., Cendak, R., Wieland, W., Alexeeff, G., 2015. Racial/ethnic disparities in cumulative environmental health impacts in California: evidence from a statewide environmental justice screening tool (CalEnviroScreen 1.1). Am. J. Public Health 105, 2341–2348.

De La Cruz-Viesca, M., Chen, Z., Ong, P.M., Hamilton, D., Darity, W.A., 2016. The Color of Wealth in Los Angeles and the Insight. Center for Community Economic Development.

Deshmukh, P., Kimbrough, S., Krabbe, S., Logan, R., Isakov, V., Baldauf, R., 2020. Identifying air pollution source impacts in urban communities using mobile monitoring. Sci. Total Environ. 715, 136979.

Di, Q., Kloog, I., Koutrakis, P., Lyapustin, A., Wang, Y., Schwartz, J., 2016. Assessing PM2.5 exposures with high Spatiotemporal resolution across the continental United States. Environ. Sci. Technol. 50, 4712–4721.

Dimanchev, E.G., Paltsev, S., Yuan, M., Rothenberg, D., Tessum, C.W., Marshall, J.D., Selin, N.E., 2019. Health co-benefits of sub-national renewable energy policy in the US. Environ. Res. Lett. 14, 085012.

Donkelaar, A. Van, Martin, R., science, C.L.-E., 2019. Regional estimates of chemical composition of fine particulate matter using a combined geoscience-statistical method with information from satellites, models, and. ACS Publ 53, 2595–2611.

Fenech, S., Doherty, R.M., Heaviside, C., Vardoulakis, S., Macintyre, H.L., O'Connor, F.M., 2018. The influence of model spatial resolution on simulated ozone and fine particulate matter for Europe: Implications for health impact assessments. Atmos. Chem. Phys. 18, 5765–5784.

Heo, J., Dulger, M., Olson, M.R., McGinnis, J.E., Shelton, B.R., Matsunaga, A., Sioutas, C., Schauer, J.J., 2013. Source apportionments of PM2.5 organic carbon using molecular marker Positive Matrix Factorization and comparison of results from different receptor models. Atmos. Environ. 73, 51–61.

Hernandez, C., Skyllakou, K., Rivera, P.G., Dinkelacker, B., Marshall, J., Pope, A., Robinson, A., Pandis, S., Adams, P., 2021. Bias Corrections for Speciated and Source-Resolved PM2.5 Chemical Transport Model Simulations Using a Geographically Weighted Regression.

Houston, D., Li, W., Wu, J., 2014. Disparities in exposure to automobile and truck traffic and vehicle emissions near the Los Angeles-long beach port complex. Am. J. Public Health 104, 156–164.

Izquierdo, R., García Dos Santos, S., Borge, R., Paz, D. de la, Sarigiannis, D., Gotti, A., Boldo, E., 2020. Health impact assessment by the implementation of Madrid City air-quality plan in 2020. Environ. Res. 183, 109021.

Jiang, X., Yoo, E. hye, 2018. The importance of spatial resolutions of Community Multiscale Air Quality (CMAQ) models on health impact assessment. Sci. Total Environ.

Joe, D.K., Zhang, H., DeNero, S.P., Lee, H.H., Chen, S.H., McDonald, B.C., Harley, R.A., Kleeman, M.J., 2014. Implementation of a high-resolution source-oriented WRF/chem model at the port of Oakland. Atmos. Environ.

Karner, A.A., Eisinger, D.S., Niemeier, D.A., 2010. Near-roadway air quality: Synthesizing the findings from Real-world data. Environ. Sci. Technol. 44, 5334–5344.

Kleeman, M.J., Cass, G.R., 2001. A 3D Eulerian source-oriented model for an externally mixed aerosol. Environ. Sci. Technol. 35, 4834–4848.

Kleeman, M.J., Zapata, C., Stilley, J., Hixson, M., 2013. PM2.5 co-benefits of climate change legislation part 2: California governor's executive order S-3-05 applied to the transportation sector. Clim. Change 117, 399–414.

Kloog, I., Chudnovsky, A.A., Just, A.C., Nordio, F., Koutrakis, P., Coull, B.A., Lyapustin, A., Wang, Y., Schwartz, J., 2014. A new hybrid spatio-temporal model for estimating daily multi-year PM2.5 concentrations across northeastern USA using high resolution aerosol optical depth data. Atmos. Environ. 95, 581–590.

Krecl, P., Cipoli, Y.A., Targino, A.C., Castro, L.B., Gidhagen, L., Malucelli, F., Wolf, A., 2020. Cyclists' exposure to air pollution under different traffic management strategies. Sci. Total Environ. 723, 138043.

Krewski, D., Jerrett, M., Burnett, R.T., Ma, R., Hughes, E., Shi, Y., Turner, M.C., Newbold, B., Ramsay, T., Ross, Z., Shin, H., Tempalski, B., 2009. Extended Follow-Up and Spatial Analysis of the American Cancer Society Study Linking Particulate Air Pollution and Mortality.

Lei, Y., Zhang, Q., He, K.B., Streets, D.G., 2011. Primary anthropogenic aerosol emission trends for China, 1990-2005. Atmos. Chem. Phys. 11, 931–954.

Lelieveld, J., Evans, J.S., Fnais, M., Giannadaki, D., Pozzer, A., 2015. The contribution of outdoor air pollution sources to premature mortality on a global scale. Nature 525, 367–371.

Li, Y., Rodier, C., Lea, J.D., Harvey, J., Kleeman, M.J., 2020. Improving spatial surrogates for area source emissions inventories in California. Atmos. Environ. 117665.

Li, Yiting, Kumar, A., Li, Yin, Kleeman, M.J., 2022. Adoption of low-carbon fuels reduces race/ethnicity disparities in air pollution exposure in California. Sci. Total Environ. 155230.

Markakis, K., Valari, M., Perrussel, O., Sanchez, O., Honore, C., 2015. Climate forced air-quality modeling at urban scale Climate forced air-quality modeling at urban scale: sensitivity to model resolution, emissions and meteorology Climate forced air-quality modeling at urban scale Climate forced air-quality modeling at urban scale. Atmos. Chem. Phys. Discuss. 15, 4767–4821.

Marshall, J.D., Swor, K.R., Nguyen, N.P., 2014. Prioritizing environmental justice and equality: diesel emissions in Southern California. Environ. Sci. Technol. 48, 4063–4068.

McDonald, B.C., McBride, Z.C., Martin, E.W., Harley, R.A., 2014. High-resolution mapping of motor vehicle carbon dioxide emissions. J. Geophys. Res. Atmos. 119, 5283–5298.

Messier, K.P., Chambliss, S.E., Gani, S., Alvarez, R., Brauer, M., Choi, J.J., Hamburg, S.P., Kerckhoffs, J., Lafranchi, B., Lunden, M.M., Marshall, J.D., Portier, C.J., Roy, A., Szpiro, A.A., Vermeulen, R.C.H., Apte, J.S., 2018. Mapping air pollution with google street view cars: efficient approaches with mobile monitoring and Land Use Regression. Environ. Sci. Technol. 52, 12563–12572.

Minet, L., Liu, R., Valois, M.F., Xu, J., Weichenthal, S., Hatzopoulou, M., 2018. Development and comparison of air pollution exposure surfaces derived from on-road mobile monitoring and Short-term stationary Sidewalk measurements. Environ. Sci. Technol. 52, 3512–3519.

Ouyang, W., Gao, B., Cheng, H., Hao, Z., Wu, N., 2018. Exposure inequality assessment for PM2.5 and the potential association with environmental health in Beijing. Sci. Total Environ. 635, 769–778.

Pan, S., Choi, Y., Roy, A., Jeon, W., 2017. Allocating emissions to 4 km and 1 km horizontal spatial resolutions and its impact on simulated NOx and O3 in Houston, TX. Atmos. Environ. 164, 398–415.

Paolella, D.A., Tessum, C.W., Adams, P.J., Apte, J.S., Chambliss, S., Hill, J., Muller, N.Z., Marshall, J.D., 2018. Effect of model spatial resolution on estimates of fine particulate matter exposure and exposure disparities in the United States. Environ. Sci. Technol. Lett. 5, 436–441.

Ramanathan, V., Carmichael, G., 2008. Global and regional climate changes due to black carbon. Nat. Geosci. 14 (1), 221–227.

Schwarzenegger, A., 2005. Executive Order S-3-05. http://static1.squarespace.com/static/549885d4e4b0ba0bff5dc695/t/54d7f1e0e4b0f0798cee3010/1423438304744/California+Executive+Order+S-3-05+(June+2005).pdf.

Seinfeld, J.H., Pandis, S.N., 2016. Atmospheric Chemistry and Physics: from Air Pollution to Climate Change, 3rd Edition. John Wiley and Sons, Hoboken, New Jersey.

Shah, R.U., Robinson, E.S., Gu, P., Apte, J.S., Marshall, J.D., Robinson, A.L., Presto, A.A., 2020. Socio-economic disparities in exposure to urban restaurant emissions are larger than for traffic. Environ. Res. Lett.

Sheppard, E., Leitner, H., Mcmaster, R.B., Tian, H., 1999. GIS-based measures of environmental equity: Exploring their sensitivity and significance. J. Expo. Sci. Environ. Epidemiol. 9, 18–28.

Su, J.G., Jerrett, M., Morello-Frosch, R., Jesdale, B.M., Kyle, A.D., 2012. Inequalities in cumulative environmental burdens among three urbanized counties in California. Environ. Int. 40, 79–87.

Tan, J., Zhang, Y., Ma, W., Yu, Q., Wang, J., Chen, L., 2015. Impact of spatial resolution on air quality simulation: a case study in a highly industrialized area in Shanghai, China. Atmos. Pollut. Res. 6, 322–333.

Tessum, C.W., Apte, J.S., Goodkind, A.L., Muller, N.Z., Mullins, K.A., Paolella, D.A., Polasky, S., Springer, N.P., Thakrar, S.K., Marshall, J.D., Hill, J.D., 2019. Inequity in consumption of goods and services adds to racial-ethnic disparities in air pollution exposure. Proc. Natl. Acad. Sci. U. S. A.

Thakrar, S.K., Balasubramanian, S., Adams, P.J., Azevedo, M.L., Muller, N.Z., Pandis, S.N., Polasky, S., Arden, C., Robinson, A.L., Apte, J.S., Tessum, C.W., Marshall, J.D., Hill, J.D., 2020. Reducing mortality from air pollution in the United States by targeting specific emission sources. Cite This Environ. Sci. Technol. Lett 7, 639–645.

Thompson, T.M., Saari, R.K., Selin, N.E., 2014. Air quality resolution for health impact assessment: influence of regional characteristics. Atmos. Chem. Phys. 14, 969–978.

Thompson, T.M., Selin, N.E., 2012. Atmospheric Chemistry and Physics Influence of air quality model resolution on uncertainty associated with health impacts. Atmos. Chem. Phys. 12, 9753–9762.

United State Census Bureau, 2020. American Community Survey (ACS) data [WWW Document]. URL. https://www2.census.gov/geo/tiger/TIGER_DP/.

US EPA, 1999. The Particle Pollution Report Current Understanding of Air Quality and Emissions through 2003 PM 2.5 Concentrations Are Declining.

Van Donkelaar, A., Martin, R.V., Brauer, M., Hsu, N.C., Kahn, R.A., Levy, R.C., Lyapustin, A., Sayer, A.M., Winker, D.M., 2016. Global estimates of fine particulate matter using a combined Geophysical-statistical method with information from satellites, models, and monitors. Environ. Sci. Technol. 50, 3762–3772.

Walker, G., 2009. Beyond distribution and proximity: exploring the multiple spatialities of environmental justice. In: Antipode. John Wiley & Sons, pp. 614–636.

Wang, T., Jiang, Z., Zhao, B., Gu, Y., Liou, K.N., Kalandiyur, N., Zhang, D., Zhu, Y., 2020. Health co-benefits of achieving sustainable net-zero greenhouse gas emissions in California. Nat. Sustain. 3, 597–605.

Yu, X., Venecek, M., Kumar, A., Hu, J., Tanrikulu, S., Soon, S.T., Tran, C., Fairley, D., Kleeman, M.J., 2019. Regional sources of airborne ultrafine particle number and mass concentrations in California. Atmos. Chem. Phys. 19, 14677–14702.

Zapata, C., Muller, N., Kleeman, M.J., 2013. PM2.5 co-benefits of climate change legislation part 1: California's AB 32. Clim. Change 117, 377–397.

Zapata, C.B., Yang, C., Yeh, S., Ogden, J., Kleeman, M.J., 2017. Low Carbon Energy Generates Public Health Savings in California. ACP.

Zhang, H., Denero, S.P., Joe, D.K., Lee, H.H., Chen, S.H., Michalakes, J., Kleeman, M.J., 2014. Development of a source oriented version of the WRF/Chem model and its application to the California regional PM10/PM2.5 air quality study. Atmos. Chem. Phys. 14, 485–503.

Zheng, B., Zhang, Q., Tong, D., Chen, C., Hong, C., Li, M., Geng, G., Lei, Y., Huo, H., He, K., 2017. Resolution dependence of uncertainties in gridded emission inventories: a case study in Hebei, China. Atmos. Chem. Phys. 17, 921–933.